TÜBİTAK

Turkish Journal of Physics

http://journals.tubitak.gov.tr/physics/

Research Article

Turk J Phys
(2016) 40: 270 – 277

doi:10.3906/fiz-1602-8

Magnetic effect on the phase properties of neodymium-activated yttrium disilicate nanomaterials

Murat ERDEM[1], **Cihat BOYRAZ**[2,*]
[1]Department of Physics, Faculty of Science and Letters, Marmara University, İstanbul, Turkey
[2]Department of Mechanical Engineering, Faculty of Technology, Marmara University, İstanbul, Turkey

Received: 10.02.2016 • **Accepted/Published Online:** 11.03.2016 • **Final Version:** 01.12.2016

Abstract: Under varying temperature conditions, undoped $Y_2Si_2O_7$ and neodymium-doped $Y_2Si_2O_7$ nanopowders were synthesized by the sol-gel method. The phase transitions from α to δ were observed in neodymium nanopowders by XRD measurements. TEM images showed ball-shaped structure forms for synthesized samples. The elemental compositions of all samples were established and quite close stoichiometry to all compound formulas was found using an attached component for TEM. To reveal the Nd dopant effect in different-phased $Y_2Si_2O_7$ nanopowders, diffuse reflectance measurements were conducted. To establish the magnetic properties of undoped $Y_2Si_2O_7$ and neodymium-doped $Y_2Si_2O_7$ nanopowders, an extensive study was carried out including M-H, M^2-H/M (Arrott's plot), and M-T under varying physical conditions. In the α phase, a significant paramagnetic increase was observed and a decrease in paramagnetic behavior was monitored by the effects of Nd dopant and increased annealing temperature.

Key words: Yttrium silicate, sol-gel, phase transition, Nd-doped yttrium silicate, and magnetic materials

1. Introduction

The host lattice of yttrium disilicate ($Y_2Si_2O_7$) shows a high refractory property, chemical stability, etc. [1]. It has been shown that the structural phases due to its complex high temperature polymorphism are in the y, z, α, β, γ, and δ forms [2]. $Y_2Si_2O_7$ investigated from a structural point was reported for the first four forms: $\alpha^{1225^\circ C} \rightarrow \beta^{1445^\circ C} \rightarrow \gamma^{1535^\circ C} \rightarrow \delta$ [3]. α-$Y_2Si_2O_7$ crystallizes into a triclinic structure with the P-1 space group and assigns four crystallographic sites to Y^{3+} ions both with six coordination numbers. β-$Y_2Si_2O_7$ crystallizes into a monoclinic structure with the $C2/_m$ space group and assigns two crystallographic sites to Y^{3+} ions both with six coordination numbers. γ-$Y_2Si_2O_7$ crystallizes into a monoclinic structure with the $P2_{1/n}$ space group and assigns two crystallographic sites to Y^{3+} ions both with six coordination numbers.

δ-$Y_2Si_2O_7$ crystallizes into an orthorhombic structure with the Pna_{21} space group and assigns unique crystallographic sites to Y^{3+} ions both with coordination number seven [4]. However, researchers focused on the optical spectroscopy properties of yttrium disilicates ($Y_2Si_2O_7$) [5–13] and no extensive study on the magnetic properties of yttrium disilicates when activated with neodymium has been observed in the literature. In this study, we first report on the magnetic properties of nanocrystalline α, γ, and δ polymorphs of yttrium disilicate ($Y_2Si_2O_7$) prepared by the sol-gel method.

*Correspondence: cboyraz@marmara.edu.tr

2. Materials and methods

Undoped and neodymium-doped nanocrystalline yttrium disilicate was synthesized in SiO_2–Y_2O_3 binary systems [14] using the sol-gel method. Precursors with the purity of 99.99% neodymium nitrate penta hydrate ($Nd(NO_3)_3{\cdot}5H_2O$), 99.999% tetraethoxysilane (TEOS,$Si(OC_2H_5)_4$), and 99.9% yttrium nitrate hexahydrate ($Y(NO_3)_3{\cdot}6H_2O$) were used to obtain the compositions. For all the samples, taken mole ratios of SiO_2 and Y_2O_3 were kept at 7.0 and the neodymium concentration was 0.025% mole in all Nd-doped samples. A detailed description of the preparation process can be found in our previous work [15]. The undoped and Nd-doped samples were then heat-treated at 1170 °C (for undoped), 1150 °C, 1250 °C, and 1480 °C for 12 h to obtain crystalline powders. XRD patterns of the annealed samples were taken with a Rigaku–XRD D-MAX 2200 with the Cu-Kα source operated with the wavelength at $\lambda = 1.5418$ Å. Slit systems, step-size (0.02°), source voltage (40 kV), and current (30 mA) were kept constant during the scans, which were conducted in θ–2θ coupled mode. Elemental compositions and the structural and morphological properties of the powders were also investigated by TEM with a JEOL JEM-2100. Diffuse reflectance spectra of the samples were obtained using a PerkinElmer Lambda 35 UV-Vis spectrophotometer to identify the absorption lines of Nd ions. Magnetic hysteresis and moment versus temperature curves of the samples were recorded by using a Vibrating Sample Magnetometer System (Quantum Design PPMS9T).

3. Results and discussion

Figure 1 presents the X-ray patterns of all powders synthesized by the sol-gel method. The phase transition of all powders was revealed under the influence of a wide annealing temperature window. Under the effect of varying annealing conditions, while the monoclinic γ-$Y_2Si_2O_7$ phase observed for the undoped sample annealed at 1170 °C, the triclinic α-$Y_2Si_2O_7$, monoclinic γ-$Y_2Si_2O_7$, and orthorhombic δ-$Y_2Si_2O_7$ phases for Nd-

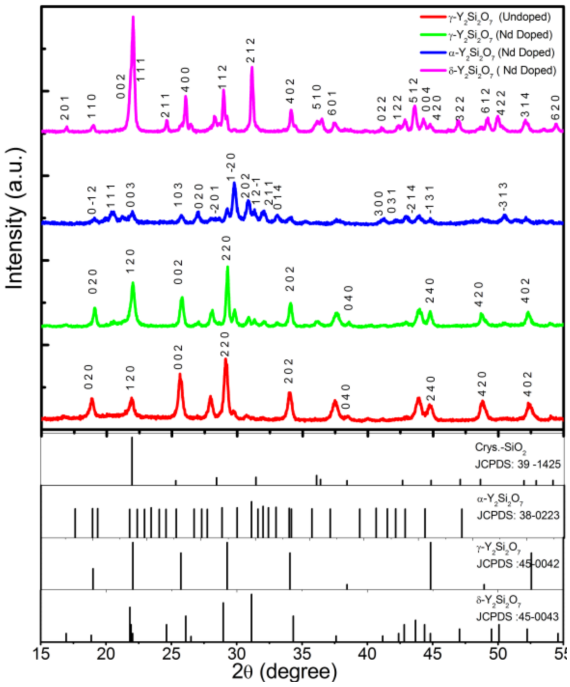

Figure 1. The X-ray patterns of all powders: α, β, γ, and δ.

doped samples were matched by comparing the peak positions and intensities with those in the Joint Committee on Powder Diffraction Standards (JCPDS) when annealed at 1150 °C, 1250 °C, and 1480 °C, respectively. It can be clearly seen that the peak positions of most of the diffraction peaks of the samples correspond well to the standard cards of α-$Y_2Si_2O_7$ (39-1425), γ-$Y_2Si_2O_7$ (45-0042), and δ-$Y_2Si_2O_7$ (45-0043), respectively. Figure 2 represents the TEM images of the undoped and Nd-doped samples with an average size change with the phase of the $Y_2Si_2O_7$ less than 100 nm. Figure 3 illustrates the EDAX spectrum of Nd-doped α-phased $Y_2Si_2O_7$ compound and the signals that indicate the existence of Y, Si, O_2, Nd, and Cu elements. The Cu signal was attributed to the copper sample holder used in the EDAX measurements.

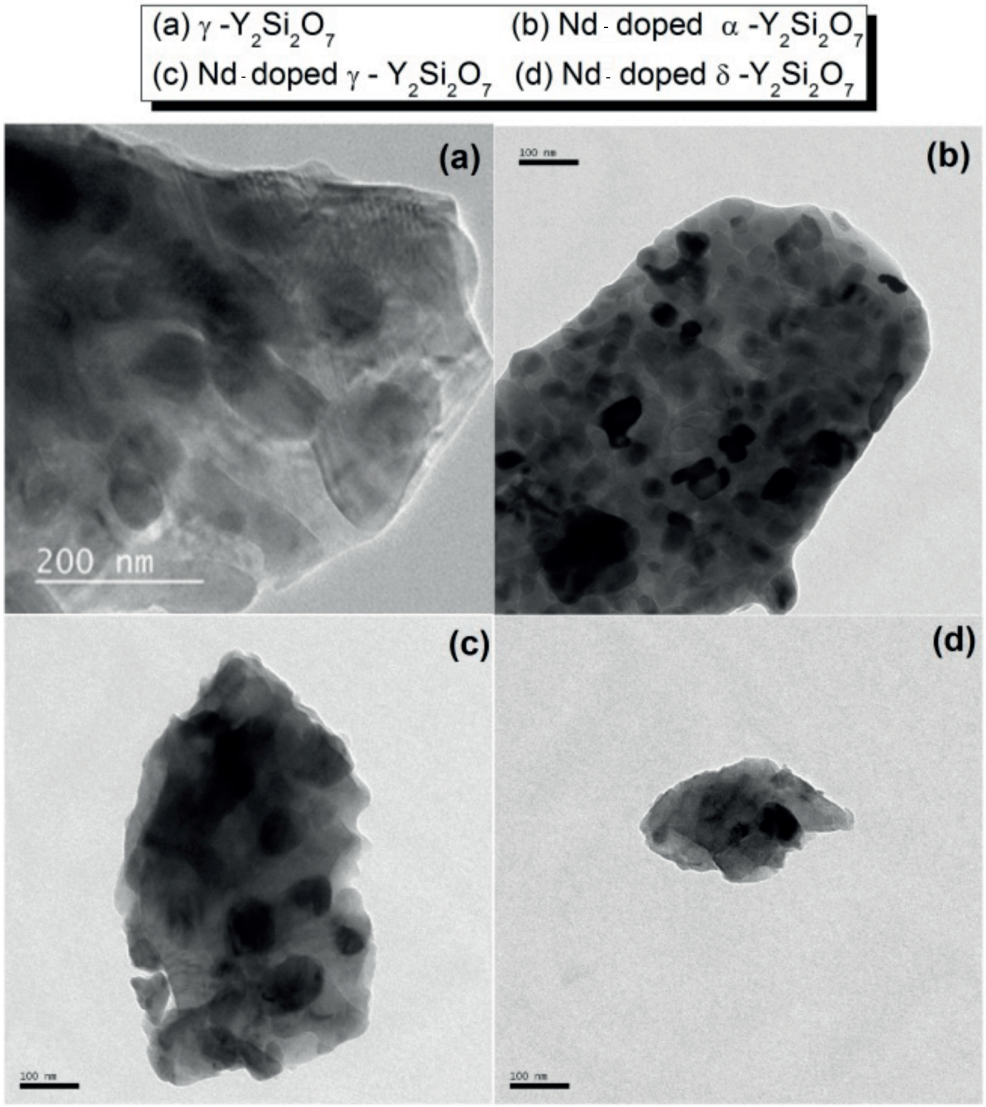

Figure 2. The TEM images of all powders.

Figure 4 displays the diffuse reflectance spectra of the undoped and Nd^{3+}-doped $Y_2Si_2O_7$ samples in the range of 450–950 nm. When Nd-doped, the reflection dips corresponding to an absorption band revealed for each phase of the samples. No indication of dip in the spectrum for the undoped $Y_2Si_2O_7$ sample was observed; thus, the Nd effect on the reflection pattern was easily observed by dips. For Nd-doped samples,

the nine dips with appreciable intensity corresponding to the observed absorption lines are due to the $f-f$ transitions from the $^4I_{15/2}$ ground level to excited levels of the Nd^{3+}. The spectral profile of the dips was slightly changing for each phase.

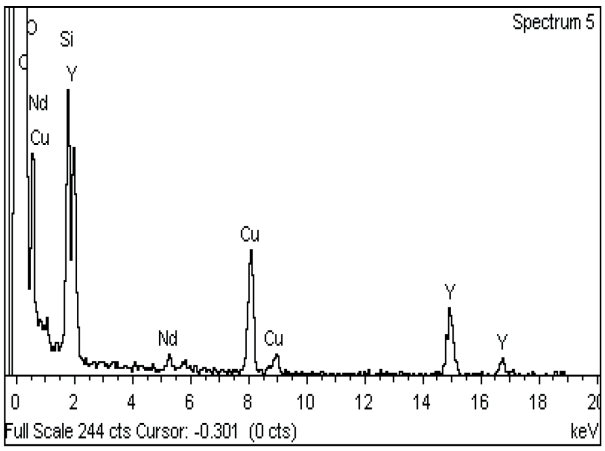

Figure 3. EDAX pattern of Nd-doped α-$Y_2Si_2O_7$ compound.

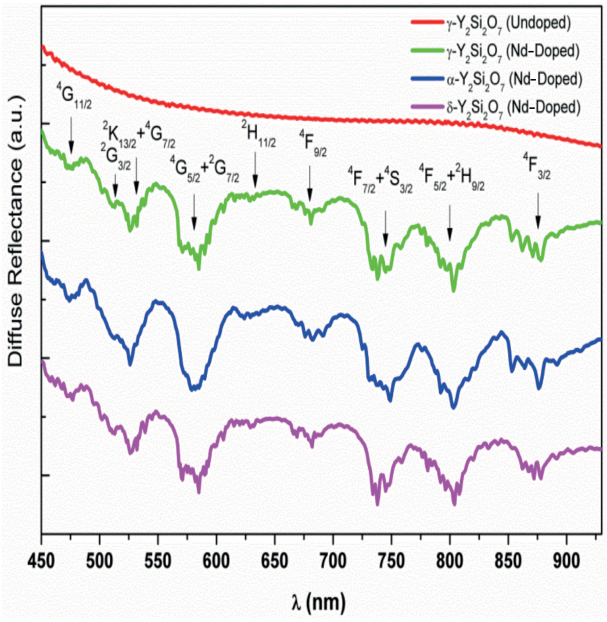

Figure 4. Wavelength and diffuse reflectance behavior of all compounds.

Figures 5a and 5b illustrate the magnetic measurements of the powders annealed at different temperatures (1150–1480 °C) to reveal the possible phase effects on the those magnetic properties. The data were taken at 10 K and 300 K, where the magnetic contributions varied with annealing temperature in a magnetic file up to ±6 kOe. The magnetic response of the powders at 10 K was observed to become 10^2 times bigger than that of the powders measured at 300 K. Local nonmagnetic phases should be predominant in the γ- and δ-phased Nd-doped $Y_2Si_2O_7$ compounds in accordance with increasing annealing temperatures. Comparing the undoped and Nd-doped α-$Y_2Si_2O_7$ compounds, a considerable paramagnetic increase can be seen in Nd-doped α-$Y_2Si_2O_7$ compounds due to the effect of the Nd dopant. The maximum magnetizations between both undoped and Nd-doped α-phased $Y_2Si_2O_7$ compounds are about 1.2 emu/g at 10 K and 0.061 emu/g at 300 K in Figures 5a and 5b. The magnetization deteriorates gradually after an annealing temperature of 1150 °C for Nd-doped samples. With the phase transition from γ to δ observed in the structure between 1250 °C and 1480 °C, the samples lose their magnetism and almost overlap each other. Similarly seen in neodymium-based magnets, Nd-doped $Y_2Si_2O_7$ compounds lose their magnetism at high temperatures, as given in Figures 5a and 5b [16,17]. We conclude that the α-phased Nd-doped $Y_2Si_2O_7$ sample has the best magnetic behavior compared to all other Nd-doped $Y_2Si_2O_7$ samples. Arrott's plots (M^2 versus H/M) of all samples given in Figures 5c–5e revealed a concave nature in all phases; this is suggestive of the antiferromagnetic nature of the investigated samples. In previous studies, similar behaviors were presented [18–20]. The $\chi^{-1}-T$ curves show a negative Curie–Weiss paramagnetic temperature for annealed samples, indicating the antiferromagnetic behavior of the samples. This should indicate the absence of ferromagnetic behavior.

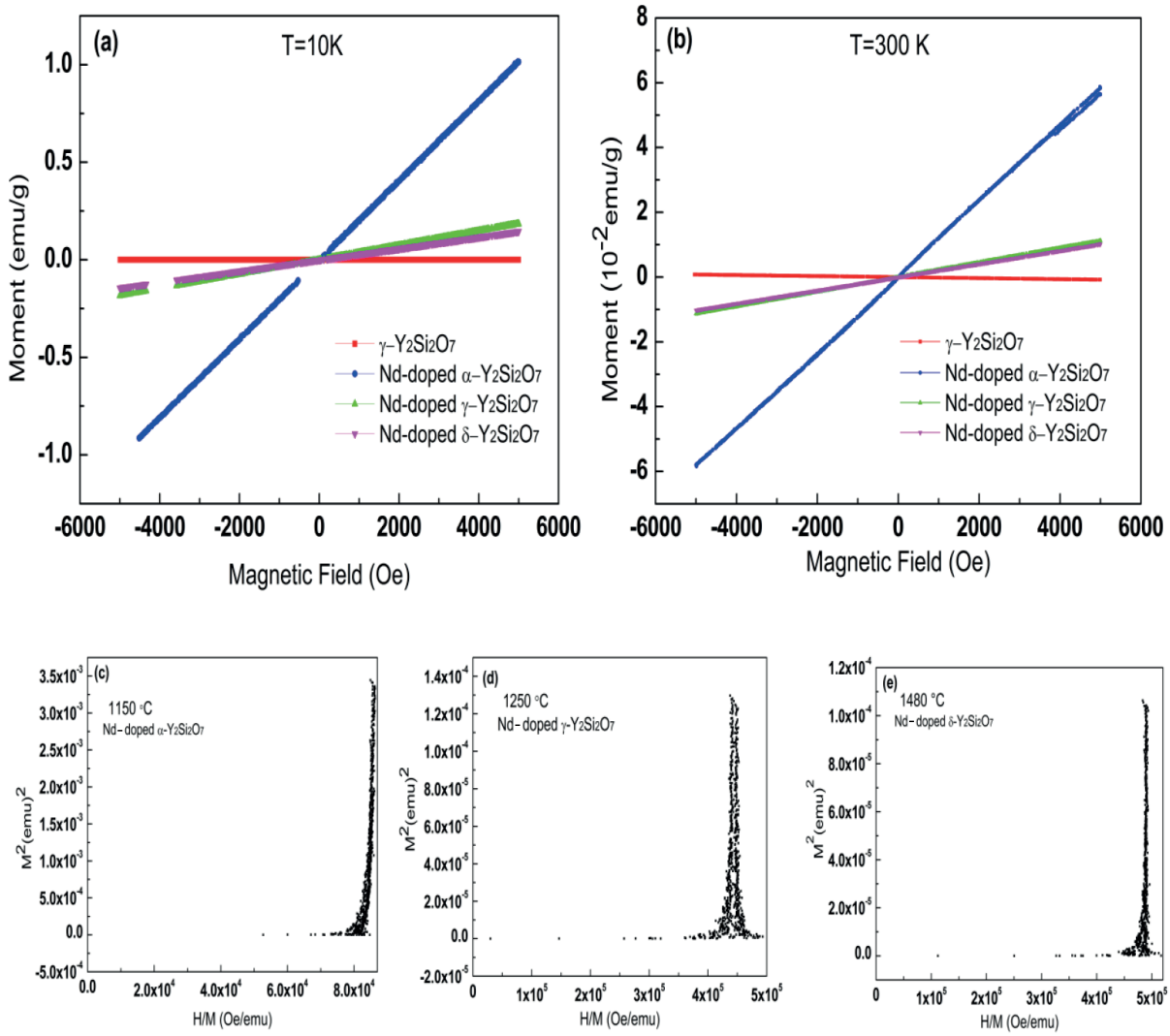

Figure 5. a) Magnetic field versus magnetic moment plot for undoped $Y_2Si_2O_7$ and Nd^{+3}-doped $Y_2Si_2O_7$ nanoparticles at 10 K; b) 10^{-2} magnetic moment at 300 K; c, d, e, and f) Arrott's plots for undoped $Y_2Si_2O_7$ and Nd^{+3}-doped $Y_2Si_2O_7$ powders annealed at different temperatures.

We have investigated the magnetic properties of $Y_2Si_2O_7$ and Nd-doped $Y_2Si_2O_7$ nanoparticles by measuring the magnetization in both zero-field cooled (ZFC) and field cooled (FC) modes under 1 kOe magnetic fields as shown in Figures 6a–6d. A slow decrease in magnetization in ZFC mode is experienced and the variation of magnetization in FC at 1 kOe exhibits a decrease at temperatures between 0 and 100 K. ZFC and FC curves, except Figure 6a, do not coincide at the temperature window of 0–300 K. The magnetization level of Nd-doped $Y_2Si_2O_7$ annealed at 1150 °C is approximately 10^2 times bigger than that of the samples annealed at 1480 °C. Similar behavior was investigated in the magnetic field versus magnetic moment measurements in Figures 5a and 5b. The inverse magnetic susceptibility (χ^{-1}) varying with temperature T for all Nd-doped samples at 1 kOe is exhibited in Figures 6e–6g. As is clearly seen in the $\chi^{-1}-T$ curves, nearly linear behavior in the temperature range of 100–300 K was observed. This is described by the Curie–Weis law.

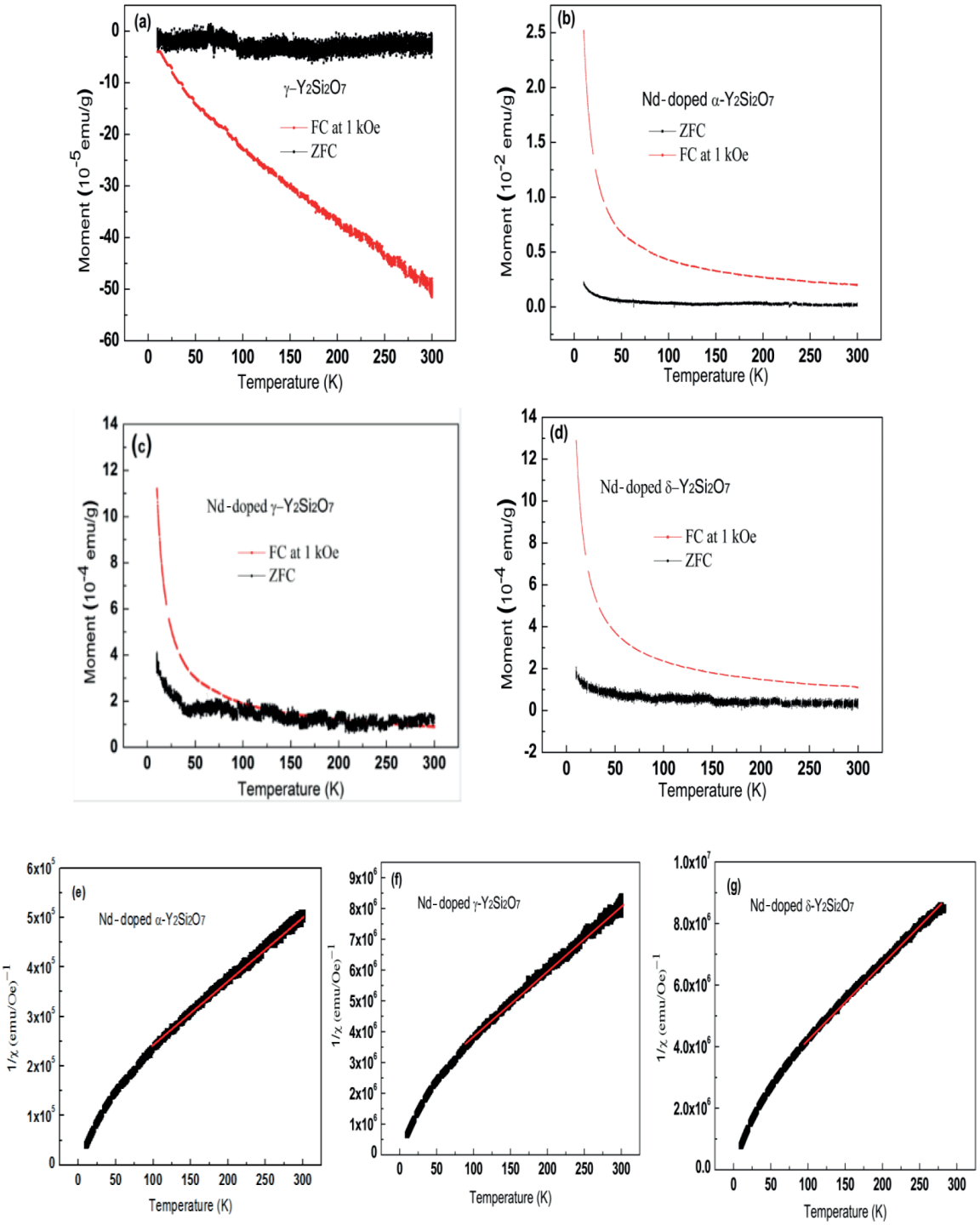

Figure 6. a) Moment versus temperature (ZFC and FC) for γ-phased $Y_2Si_2O_7$ at 1170 °C; b, c, and d) ZFC and FC for α-, γ-, and δ-phased Nd-doped $Y_2Si_2O_7$ at 1150 °C, 1250 °C, and 1480 °C. respectively; e, f, and g) $\chi^{-1}-T$ plots (negative Curie–Weiss paramagnetic temperature) for all Nd-doped samples.

The effects of Nd dopant and annealing temperature on the magnetic moment of undoped and Nd-doped $Y_2Si_2O_7$ nanopowders are clearly seen in Figure 7. A decrement was observed after α-phased maximum

magnetic moment monitored at 1150 °C so the Nd dopant effect is a possible reason for the varying magnetic moment value. In Nd-doped $Y_2Si_2O_7$ samples, the magnetic moment values decrease slightly after approximately 1250 °C. The reasons behind this might be temperature-dependent phase transition, namely the decrease in magnetization that is actively seen with the increment of annealing temperature, and, like neodymium-based magnets, the Nd-doped $Y_2Si_2O_7$ compound loses its magnetism at high temperatures [18,21]. This should be an indication of increasing local nonmagnetic regions and an increase in random spin orientation in the structure. A slight difference in magnetic moment values was observed between γ-$Y_2Si_2O_7$ and Nd-doped δ-$Y_2Si_2O_7$, in which the Nd dopant effect on magnetization almost disappears at 1480 °C annealing temperature.

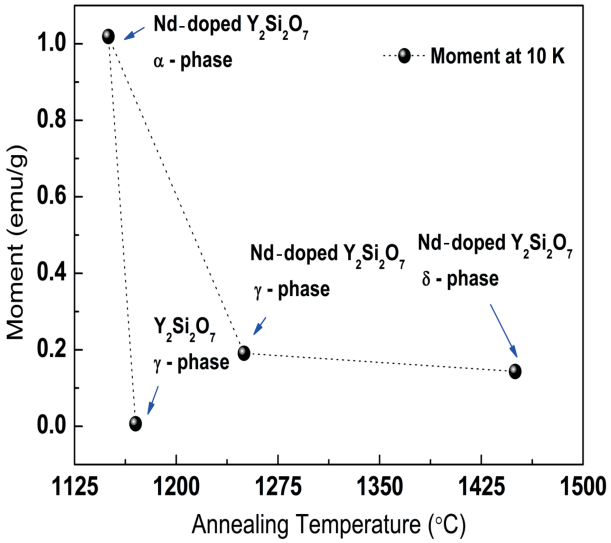

Figure 7. Annealing temperature versus magnetic moment plot for undoped $Y_2Si_2O_7$ and Nd^{+3}-doped $Y_2Si_2O_7$ nanoparticles at 10 K.

4. Conclusion

We have investigated structural and magnetic properties of undoped $Y_2Si_2O_7$ and Nd-doped $Y_2Si_2O_7$ nanoparticles annealed at varying temperature conditions. It was found that, structurally and magnetically, the $Y_2Si_2O_7$ compound was affected by Nd dopant and increasing annealing temperature. The phase transitions $\alpha \rightarrow \gamma$ and $\gamma \rightarrow \delta$ were revealed by XRD measurements. A ball-shaped structure was formed, as shown in TEM images. Comparing the undoped and Nd-doped α-$Y_2Si_2O_7$ compounds, a considerable paramagnetic increase can be seen in the Nd-doped α-$Y_2Si_2O_7$ compound due to Nd dopant effect. Nd-doped $Y_2Si_2O_7$ powders lost their magnetisms at high temperatures so this should be a reason for the increasing local nonmagnetic regions and an increase in random spin orientation in the structure. In ZFC mode, a slow increase in magnetization was experienced and in FC mode at 1 kOe the variation of magnetization exhibits a decrease in the temperature between 0 and 100 K. The phase transition depending on annealing temperature has been well established.

Acknowledgment

This work was financially supported by the Scientific Research Projects Department (BAPKO) of Marmara University with project number FEN-B-150513-0170 and project number FEN-E-100713-0319.

References

[1] Dolan, M.D.; Harlan, B.; White, J.S.; Hall, M.; Misture, S.T.; Bancheri, S.C.; Bewlay, B. *Powd. Diff.* **2008**, *23*, 20-25.

[2] Felsche, J. *Structure and Bonding* **1973**, *13*, 99-197.

[3] Becerro, A. I.; Escudero, A.; Florian, P.; Massiot, D.; Alba, M. D. J. *Sol. Sta. Chem.* **2004**, *177*, 2783-2789.

[4] Becerro, A. I.; Escudero, A. *Phase Trans.* **2004**, *77*, 1093-1102.

[5] Erdem, M.; Ozen, G.; Tav, C.; Bartolo, B. D. *Ceram. Int.* **2013**, *39*, 6029-6033.

[6] Erdem, M.; Ekmekci, M. K.; Orucu, H.; Bilir, G. *Int. J. Appl. Cer. Tec.* **2015**, *12*, 1-4.

[7] Zhou, P.; Yu, X.; Yang, L.; Yang, S.; Gao, W. *J. Lumin.* **2007**, *124*, 241-244.

[8] Erdem, M.; Sitt, B. *Opt. Mat.* **2015**, 46, 260-264.

[9] Hreniak, D.; Gluchowski, P.; Strek, W.; Bettinelli, M.; Kozlowska, A.; Kozlowski, M. *Mater. Sci.* **2006**, *24*, 405-413.

[10] Erdem, M.; Eryurek, G.; Mergen, A.; Di Bartolo, B. *Ceramics Int.* **2016**, 42, 1501-1506.

[11] Marciniak, L.; Hreniak, D.; Dobrowolska, A.; Zych, E. *Appl. Phys. A*. **2010**, *99*, 871-877.

[12] Erdem, M.; Eryurek, G.; Di Bartolo, B. *Opt. Mat.* **2015**, 49, 90-93.

[13] Erdem, M.; Eryurek, G.; Di Bartolo, B. *J. All. Comp.* **2015**, 639, 483-487.

[14] Chambers, J. J.; Parsons, G. N. *J. Appl. Phys.* **2001**, *90*, 918-933.

[15] Erdem, M.; Özen, G.; Tav, C. *J. Euro. Cer. Soc.* **2011**, *31*, 2629-2631.

[16] Hirosawa, S.; Matsuura, Y.; Yamamoto, H.; Fujimura, S.; Sagawa, M.; Yamauchi, H. *J. Appl. Phys.* **1986**, *59*, 873-913.

[17] Sagawa, M.; Fujimura, S.; Togawa, N.; Yamamoto, H.; Matsuura, Y. *J. Appl. Phys.* **1984**, *55*, 2083-2087.

[18] Croat, J. J.; Herbst, J. F.; Lee, R. W.; Pinkerton, F. E. *J. Appl. Phys.* **1984**, *55*, 2072-2078.

[19] El-Hagary, M.; Soltanb, S. *Solid State Commun.* **2013**, *155*, 29-33.

[20] Venkatesan, M.; Fitzgerald, C. B.; Lunney, J. G.; Coey, J. M. D. *Phys. Rev. Lett.* **2004**, *93*, 177206-4.

[21] Fraden, J. *Handbook of Modern Sensors: Physics, Designs, and Applications*, 4th ed.; Springer: New York, NY, USA, 2010.